ACS OMEGA

http://pubs.acs.org/journal/acsodf

Article

Efficient Synergistic Antibacterial Activity of α-MSH Using Chitosan-Based Versatile Nanoconjugates

Sourav Barman,[⊥] Asmita Chakraborty,[⊥] Sujata Saha, Kunal Sikder, Sayoni Maitra Roy, Barkha Modi, Sabarnee Bahadur, Ali Hossain Khan, Dipak Manna, Pousali Bag, Ankan Kumar Sarkar, Rishi Bhattacharya, Arnab Basu,* and Amit Ranjan Maity*

Cite This: *ACS Omega* 2023, 8, 12865−12877

Read Online

ACCESS | Metrics & More | Article Recommendations | Supporting Information

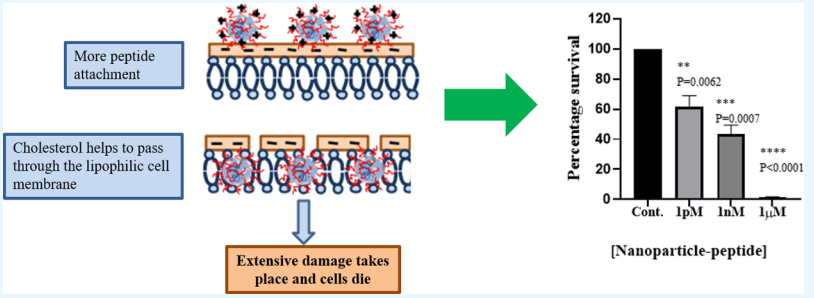

ABSTRACT: The application of antimicrobial peptides has emerged as an alternative therapeutic tool to encounter against multidrug resistance of different pathogenic organisms. α-Melanocyte stimulating hormone (α-MSH), an endogenous neuropeptide, is found to be efficient in eradicating infection of various kinds of *Staphylococcus aureus*, including methicillin-resistant *Staphylococcus aureus* (MRSA). However, the chemical stability and efficient delivery of these biopharmaceuticals (i.e., α-MSH) to bacterial cells with a significant antibacterial effect remains a key challenge. To address this issue, we have developed a chitosan-cholesterol polymer using a single-step, one-pot, and simple chemical conjugation technique, where α-MSH is loaded with a significantly high amount (37.7%), and the final product is obtained as chitosan-cholesterol α-MSH polymer−drug nanoconjugates. A staphylococcal growth inhibition experiment was performed using chitosan-cholesterol α-MSH and individual controls. α-MSH and chitosan-cholesterol both show bacterial growth inhibition by a magnitude of 50 and 79%, respectively. The killing efficiency of polymer−drug nanoconjugates was very drastic, and almost no bacterial colony was observed (∼100% inhibition) after overnight incubation. Phenotypic alternation was observed in the presence of α-MSH causing changes in the cell structure and shape, indicating stress on *Staphylococcus aureus*. As a further consequence, vigorous cell lysis with concomitant release of the cellular material in the nearby medium was observed after treatment of chitosan-cholesterol α-MSH nanoconjugates. This vigorous lysis of the cell structure is associated with extensive aggregation of the bacterial cells evident in scanning electron microscopy (SEM). The dose-response experiment was performed with various concentrations of chitosan-cholesterol α-MSH nanoconjugates to decipher the degree of the bactericidal effect. The concentration of α-MSH as low as 1 pM also shows significant inhibition of bacterial growth (∼40% growth inhibition) of *Staphylococcus aureus*. Despite playing an important role in inhibiting bacterial growth, our investigation on hemolytic assay shows that chitosan-cholesterol α-MSH is significantly nontoxic at a wide range of concentrations. In a nutshell, our analysis demonstrated novel antimicrobial activity of nanoparticle-conjugated α-MSH, which could be used as future therapeutics against multidrug-resistant *Staphylococcus aureus* and other types of bacterial cells.

1. INTRODUCTION

The increased incidence of antibiotic resistance necessitates the need for the development of novel antimicrobials that could be effectively treated against disease-producing pathogens. Various pharmaceuticals/drugs, e.g., small molecule drugs and biopharmaceutics have been used traditionally as an alternative therapy against antibiotic treatment to combat the growth and virulence of different organisms. One such very popular method is the application of antimicrobial peptides (AMPs). This particular group of small biomolecules gained recent scientific attention as a potential antimicrobial agent because of its unique mode of action (MOA) which differs from traditional antibiotics.[1] AMPs are produced from a variety of species[2] and destroy a broad spectrum of

Received: December 27, 2022
Accepted: March 20, 2023
Published: March 30, 2023

microorganisms.[3] The action mechanism of AMPs is either by disrupting the cell membrane and fostering the subsequent leakage of cellular materials or by interfering with the regular metabolic functions by binding with protein or nucleic acid.[4,5] This AMP-based cellular destruction of organism method has been gaining popularity, and chemical/structural modification over native AMP has ensured better efficacy and enhanced stability inside the cellular environment.

Alpha-melanocyte stimulating hormone (α-MSH) is an endogenous neuropeptide with linear tridecapeptides (Ac-Ser^1-Tyr^2-Ser^3-Met^4-Glu^5-His^6-Phe^7-Arg^8-Trp^9-Gly^{10}-Lys^{11}-Pro^{12}-Val^{13}-NH_2) that results from the cleavage of its precursor polypeptide pro-opiomelanocortin (POMC).[6] Besides its melanogenic properties, it is also known for its antipyretic and anti-inflammatory effects.[7] At the molecular level, they interact with the melanocortin receptor (MC1R, MC3R, MC4R), thereby interfering with the cAMP signaling through the downregulation of NF-$\kappa\beta$ and protecting the brain and peripheral organs from inflammatory conditions. Apart from its physiological function, α-MSH exhibits potential lethal activity against Gram-positive bacteria especially *Staphylococcus aureus*, vindicating its bactericidal properties.[8] The bactericidal activity is observed at the C-terminal end as truncated peptides also show bactericidal effects. A modified version of peptide palmitoylated α-MSH has shown to be highly effective against the highly resistant biofilm of *Staphylococcus aureus*. Pal-α-MSH[9−11] emerged as the most effective AMP as palmitoylation led to a remarkable enhancement in its activity against stationary phase bacteria.[12]

Although the nature and concentration of different inhibitory molecules are crucial for the prevention of bacterial growth, effective delivery of these molecules to their target site of action is also very important to achieve an efficient pharmacological effect. Fortunately, recent advancements in nanobiotechnology have enabled us with various nanocarriers that can efficiently target the pharmaceutics to their target site of action in a wide range of areas, from tumor cells[13−20] to bacterial cells.[21] The wide possibilities of either encapsulation or chemical modifications of drugs into the nanocarrier, precise control over its size, decorating its surface with disease-targeting ligands that facilitate the interaction between loaded drugs and target cells, and the efficient drug release mechanism made it one of the most promising tools for conjure therapeutic benefits. These benefits of nanocarriers are not only restricted in the area of tumor-targeted drug therapy[22] but also have a remarkable effect on a wide range of bacteria. The colossal surface-area-to-volume ratio of this system increases the contact points with different organisms and therefore helps in drug delivery.[23] Nanocarriers demonstrated antibacterial properties in various ways: by membrane perturbation, interfering with metabolic processes, damaging cellular components, producing reactive oxygen species, inhibiting protein and RNA synthesis, etc.[24] The antibacterial properties of nanocarriers highly depend on their physical and chemical characteristics (e.g., size, surface charge, drug-loading efficiency, shape, presence and nature of targeting ligands, etc.).[25,26] and these tunable properties provide selective advantages in the context of drug loading and releasing to the target site without losing chemical stability of the complex.

A nanocarrier that is easy to synthesize, efficient in bioconjugation, and has drug-loading ability with versatile implications is a promising candidate in the aspect of translational research and development for bench-to-bedside applications.[22,27] There are many inorganic and organic nanocarriers known so far that have potential antibacterial properties.[28] Interestingly, chitosan-based biopolymers have emerged as an attractive potent antibacterial agent against various bacteria like *E. coli* and *S. aureus*.[29] Modified chitosan with certain metal ions and antibiotics have been proven to be efficient against fungus *Cryptococcus neoformans* (*C. neoformans*), *Candida albicans* (*C. albicans*), and Gram-negative *Pseudomonas aeruginosa* (*P. aeruginosa*) and MDR *S. aureus*.[30−32] Chitosan derivatives have exhibited their bactericidal action against biofilms of *S. aureus* and *S. mutants*.[33,34] Although the exact mechanism of highly efficacious antibacterial activity of chitosan is yet to be understood, it is well known that the antibacterial activity of chitosan is based on a number of intrinsic and extrinsic factors.[35] Intrinsic factors include the molecular weight and degree of deacetylation of parent chitosan, size and concentration of nanocarriers, etc.[36] The extrinsic factors include pH, temperature, etc.[22] The mechanism includes binding of chitosan to the negatively charged bacterial cell wall, causing altering of the cell surface permeability.[37] Loss of cellular permeability renders the leakage of cytoplasmic contents in extracellular space, leading to cell death.[38] Besides its polycationic structures, the antibacterial effect is also exerted through the generation of membrane instability by chelating essential ions such as Mg^{2+} and Ca^{2+} that influence the integrity of cell walls and degradative enzymes.[39−42] Cholesterol is another active ingredient, which is routinely used in the preparation of nanopolymers. This vital structural and functional cellular component is frequently used to alter hydrophobicity of biomaterials and form suitable complex structures using its hydrophobic feature.[43]

In this article, we modified the low molecular weight and water-soluble chitosan with cholesterol using a single-step, one-pot, simple chemical method to produce chitosan-cholesterol nanocarriers. The physical loading of α-MSH helps to form the chitosan-cholesterol α-MSH polymer−drug nanoconjugates that can more efficiently adhere and pass through the cell wall of Gram-positive methicillin-resistant *Staphylococcus aureus* (MRSA) (Scheme 1). We have successfully demonstrated in vitro bactericidal activity of the compound that is efficient enough to kill almost 100% of bacterial cells. Moreover, we confirmed that the effect of the chitosan-cholesterol α-MSH polymer−drug nanoconjugates exists till the limit of the picomolar concentration. Based on the interesting results obtained from this study, it can be said that our simple but versatile chitosan-based nanocarrier system has the potential to be an efficient alternative therapy against different clinically important organisms.

2. EXPERIMENTAL SECTION

2.1. Materials. Chitosan oligosaccharide ($M_n \sim 5000$ Da) was purchased from TCI chemicals and cholesteryl chloroformate (95%) from Sigma Aldrich. Dimethyl sulfoxide (DMSO), diethyl ether, dichloromethane, and *N*,*N*-dimethylacetamide (DMA) were procured from Merck and Rankem. Triethylamine (TEA) and Resazurin were purchased from TCI chemicals. Dialysis membranes (MWCO 2000 and 12,000 Da) and MTT were purchased from Sigma Aldrich. α-MSH (EEEDDDSYSMEHFRWGKPV) was purchased from S Biochem. The USA300 MRSA strain has been used to perform all kinds of experiments. All the chemicals were used as received.

https://doi.org/10.1021/acsomega.2c08209
ACS Omega 2023, 8, 12865−12877

Scheme 1. Chitosan-Cholesterol α-MSH Preparation and Its Interactions with Bacteria Cells[a]

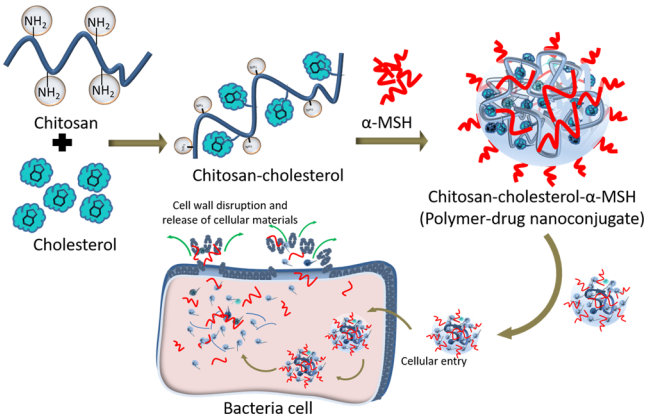

[a]The polymer−drug nanoconjugates of α-MSH were prepared by reaction between chitosan and cholesterol units, interacted with bacteria cell walls, made it more permeable, and finally disrupted the cell wall and released cellular materials, leading to inhibition of bacterial cell growth and death.

2.2. Instrumentation. An Olympus CKX53 instrument and an Olympus BX53 microscope were used for performing bright field, DIC, and fluorescence imaging. A Hitachi U-2910 UV−visible spectrophotometer was used for measuring UV−visible absorption spectra, using a quartz cell of 1 cm path length. A Hitachi F-4600 spectrophotometer was used for measuring fluorescence spectra. Size distribution and surface charge analysis via dynamic light scattering (DLS) were quantified using a Nano ZS (Malvern) instrument. Hemolytic analysis was performed using a multiplate reader (PerkinElmer Victor Nivo).

2.3. Synthesis of Chitosan-Cholesterol. Chitosan-cholesterol was synthesized using our previous method with some modifications.[44] Briefly, the chitosan oligosaccharide (i.e., chitosan) was dissolved in DMSO (300 mg, 0.06 mmol in 7 mL DMSO), and 120 μL of triethylamine was added to it. Then, cholesteryl chloroformate (215 mg, 0.48 mmol) was dissolved in 7 mL of DMA and added gradually to chitosan solution with continuous stirring at room temperature. Reaction continued overnight (Figure 1). Then, the product chitosan-cholesterol was separated from unreacted reagents using the ether precipitation method. Briefly, the reaction mixture was added dropwise to cold diethyl ether and centrifugation of the mixture was done at 6000 rpm for 5 min. The same process was repeated a few times. The chitosan-cholesterol was collected in the form of a precipitate. Finally, the chitosan-cholesterol polymer was thoroughly washed with dichloromethane to remove any excess cholesteryl chloroformate, solvents etc.; finally, it was dried well and stored at 4 °C to use further whenever needed.

2.4. Preparation of Chitosan-Cholesterol α-MSH Polymer−Drug Nanoconjugates. To prepare chitosan-cholesterol α-MSH polymer−drug nanoconjugates, we used α-MSH peptide drug (M_W ∼ 2395 Da) and chitosan-cholesterol polymer. Chitosan-cholesterol was dissolved (122 mg, 0.022 mmol) in water and α-MSH (3.5 mg, 1.46 mmol) was dissolved in DMSO. Then, the α-MSH solution was added dropwise to chitosan-cholesterol solution at room temperature under constant, slow stirring and continued for 2 days. After α-MSH loading, the solution was dialyzed overnight against double-distilled water using a dialysis membrane (MWCO 12,000 Da) to remove DMSO and any free α-MSH.

2.5. Calculation of α-MSH Loading in Chitosan-Cholesterol α-MSH Polymer−Drug Nanoconjugates. The calibration curve of α-MSH was prepared using several diluted solutions of α-MSH in water and absorbance values at 280 nm wavelength for α-MSH. α-MSH [1.25 mg (0.52 mmol)] was dissolved in 5 mL of distilled water which made a dilution series and absorbance values were obtained using a UV−visible absorption spectrometer. The drug-loading percentage was calculated from the calibration curve (Abs = 0.263Conc.), with absorbance value 0.066 using the following equation.

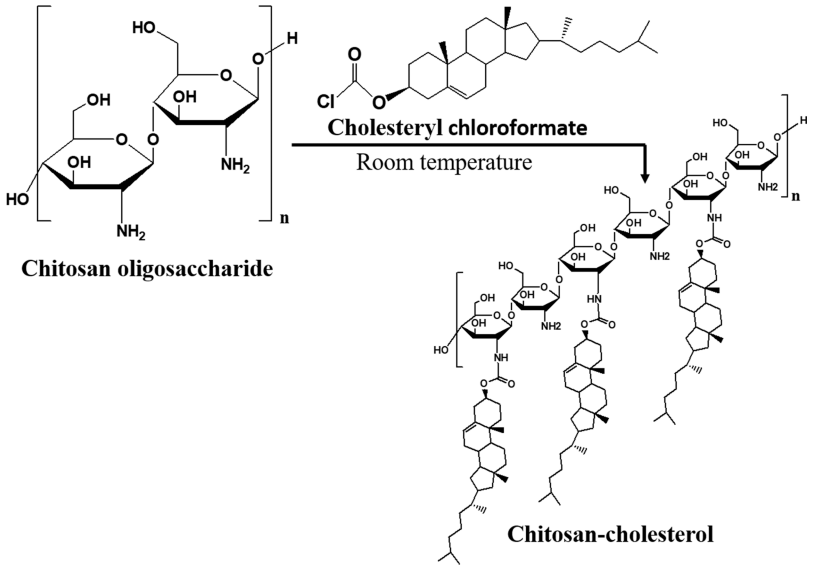

Figure 1. Synthesis of chitosan-cholesterol. The graft polymer used in this study was synthesized by modification of the chitosan backbone with cholesterol units using a single, one-pot chemical conjugation strategy and used for further α-MSH loading.

https://doi.org/10.1021/acsomega.2c08209
ACS Omega 2023, 8, 12865−12877

$$\text{Drug} - \text{loading percentage} = (\text{final concentration of the drug/initial concentration of the drug}) \times 100\%$$

2.6. Bactericidal Assay for the Antimicrobial Study of Chitosan-Cholesterol α-MSH. The bactericidal assay was performed according to the protocol mentioned earlier. Briefly, *Staphylococcus aureus* bacterial cells were grown overnight and freshly inoculated into 50 mL tryptic soy broth (TSB) medium in 1:100 ratio and allowed to grow up to mid-exponential phase (OD_{600} = 0.5). The bacterial cells were harvested and washed with phosphate buffer saline (1× PBS) and serially diluted to 10^5 numbers of cells. All sets of components used in our analysis (such as α-MSH, chitosan-cholesterol polymer and polymer−drug nanoconjugates) have been administered in a concentration of 1 μM in 100 μL total volume. The reaction was carried out at 37 °C for two hours. A volume of 50 μL was taken from the reaction mixture and plated on tryptic soya agar (TSA). The plates were incubated overnight, and different numbers of colonies appeared on each plate. The number of colonies was enumerated and analyzed. The result was interpreted with respect to control where no treatment has been done. The result was compared with the control which was not treated with different components.[45]

2.7. SEM Study. The bacterial cell culture was prepared in the same way as the bactericidal analysis was performed. The bacterial cells were grown up to the mid-exponential phase and washed thrice with 10 mM PBS and diluted in the same buffer to OD_{600} = 1.0 (cell number 10^9). The concentrations of the α-MSH peptide and chitosan-cholesterol α-MSH were kept at 30 μM. After two hours of incubation at 37 °C, cells were removed by centrifuging at 6000 rpm for 10 min. The cells were washed with 10 mM PBS (pH 7.5) thrice to get rid of all kinds of salts associated with them. Glutaraldehyde (2.5%) was used to fix the bacterial cell at 4 °C overnight. On the next day, the fixed cells were again collected by centrifugation at 6000 rpm for 10 min and washed with 10 mM PBS again to wash out the excess fixative from it. SEM analysis was performed on Quanta FEG 250 operating at an accelerating voltage of 20 kV. Silicon wafers were used to prepare SEM specimens. For each sample, a droplet of bacterial suspension was cast on a silicon wafer and dried overnight in a vacuum desiccator. The gold coating was done before inserting the samples into the microscope.

2.8. Hemolytic Analysis of Chitosan-Cholesterol α-MSH. Hemolytic analysis was done using fresh human blood. Briefly, the collected blood was gently centrifuged at 1500 rpm for 10 min to remove the plasma, and the collection of red blood cells (RBCs) was done without being hemolyzed. RBCs were washed with 10 mM PBS twice and resuspended in the same buffer. An aliquot of 100 μL of RBC suspension was added to different concentrations of chitosan-cholesterol α-MSH diluted in 100 μL of PBS buffer. The mixture was incubated at 37 °C for one hour and centrifuged again in order to get the supernatant. The absorbance of the supernatant was measured at 414 nm using a 96-well plate in a multiplate reader (PerkinElmer Victor Nivo). Triton X-100 (1%) was used to measure 100% lysis of RBCs used as the positive control. Similarly, hemolysis was done with PBS used as the negative control (0% lysis). The percentage of hemolysis was calculated from the following equation.

$$\%\text{hemolysis} = (\text{OD of sample} - \text{OD of PBS})/(\text{OD of positive control} - \text{OD of PBS}) \times 100$$

2.9. Bacterial Growth Analysis in the Presence of Polymer−Drug Nanoconjugates. Overnight-grown saturated culture of MRSA was inoculated in TSB in 1:100 ratio, and the growth was monitored in the presence of different concentrations of chitosan-cholesterol α-MSH. The optical density of the culture at 600 nm wavelength from different time points illustrates the growth profile of the organism. In order to see the bactericidal effect of the chitosan-cholesterol α-MSH, samples have been added either in the beginning or after reaching mid-exponential phase of growth (OD_{600} = 0.5). The concentration of the polymer−drug nanoconjugates was kept similar in both the cases. Colony forming units (CFUs) were calculated from the culture of two different timepoints, where a visible difference in absorbance was observed. The difference in the number of CFU encompasses the relative abundance of the live cells in the culture, therefore synonymous of the growth of the organism at that point.

2.10. Determination of the MIC. Determination of the minimum inhibitory concentration (MIC) is important since it gives an idea of the effective dosage of chemotherapeutics. With a view to know the MIC of the polymer−drug nanoconjugates, different concentrations of samples (up to 5 μM) were mixed with the growing culture of MRSA in a series of experimental sets. The growth of the organism was determined by measuring absorbance (OD_{600}) after overnight incubation and the concentration of chitosan-cholesterol α-MSH in which growth is completely inhibited is the MIC of chitosan-cholesterol α-MSH (Figure S4).

2.11. Microscopic Differentiation of Live and Dead Cells by Trypan Blue Staining. The effect of the polymer−drug nanoconjugates can be illustrated by trypan blue staining. This particular stain specifically colors the internal part of the dead cell, but in the case of the live cell, only the membrane gets stained. Briefly, the MRSA cells in the mid-log phase have been harvested and washed with PBS buffer. The cell suspension is treated with 30 μM of polymer−drug nanoconjugates for two hours at 37 °C. A set of MRSA which was not treated with the conjugates remained as the control. The treated cells were washed twice with the PBS buffer and mixed with trypan blue for staining. The stained cells were put inside a coverslip and observed under bright field with 40× magnification.

2.12. Membrane Perforation Analysis by Wheat Germ Agglutinin Staining. The effect of polymer−drug nanoconjugates on the cell membrane of MRSA has been illustrated with this particular staining procedure. Briefly, MRSA cells are harvested from the mid-log phase and washed with PBS 7.4 buffer. The cells were treated with 30 μM of polymer−drug nanoconjugates for two hours at 37 °C. The cells without treatment were set as the control. Cells are harvested after the treatment and washed again with PBS. Paraformaldehyde (PFA) solution (4%) is applied for 30 min under room temperature to fix the cell. Once the cells were fixed, the PFA solution was washed out with repeated washing and the cells were stained with wheat germ agglutinin (WGA) that specifically stain the membrane of the cell. Excess stain was removed by washing, and the cell suspension is put on the coverslip and air-dried. The coverslip was mounted with a gold

https://doi.org/10.1021/acsomega.2c08209
ACS Omega 2023, 8, 12865−12877

antifade mounting agent and observed under fluorescence microscopy using 100× magnification.

2.13. Cell Viability Determination by Resazurin Dye. Cell viability was determined by performing the resazurin experiment. Resazurin is a substrate that changes color in response to metabolic activity. The reduction of resazurin gives rise to pink-colored fluorescent product resorufin. The dye is most frequently used for the determination of cellular viability of bacterial and eukaryotic cells. In this particular analysis, we performed the treatment of chitosan-cholesterol-αMSH on the *Staphylococcus aureus* as previously mentioned, and the cells are washed with 1× PBS twice and resuspended in the same buffer. This is followed by the addition of the resazurin, and the mixture was incubated at room temperature for one hour. Visible color change has been observed in the control where no treatment was done. The color of the samples treated with 1 and 30 μM of the chitosan-cholesterol-αMSH remained unchanged due to the absence of viable cells (Figure S6).

2.14. Measuring Cytotoxicity by MTT Assay. The viability of HT22 skin cancer cells was determined through the MTT assay to evaluate the cytotoxicity of peptides, as described previously.[44] The cell line was prepared in 24-well plates (~5×10^5 cells per well) in DMEM supplemented with 10% FBS and suitable antibiotics at 37 °C with 5% CO_2. After overnight, various concentrations of chitosan-cholesterol α-MSH were added to each well (in triplicate). The cells with medium and without the sample was as negetive control. The plate was incubated for 2 h at 37 °C. The MTT solution (0.1 mg mL^{-1}) was added to each well, and the plates were again incubated for 3 h at 37 °C. Subsequently, after carefully removal of the supernatants, 200 μL of dimethyl sulfoxide was then added to each well and shaken well to dissolve the formazan crystals formed, and absorbance was measured at 570 nm. The assay was done in triplicate on three different days, and the percentage of cytotoxicity was determined using the following equation.

$$\%\text{cytotoxicity} = [(\text{OD of negative} - \text{control OD of sample})]/(\text{OD of negative control}) \times 100$$

3. RESULTS

3.1. Characterization of Chitosan-Cholesterol. We have characterized chitosan-cholesterol graft copolymer by Fourier transform infrared (FTIR) spectroscopy and matrix-assisted laser desorption/ionization time-of-flight mass spectroscopy (MALDI-TOF-MS). The characteristic peak of N−H bending at 1519 and 1637 cm^{-1} of the primary amine in chitosan shifted to 1552 and 1652 cm^{-1}, respectively, of amide in chitosan-cholesterol. The stretching vibration of C═O at 1770 cm^{-1} of the carbonyl group in cholesteryl chloroformate is present at 1739 cm^{-1} in chitosan-cholesterol. Moreover, peaks at 1465 cm^{-1} for C−H bending and 2949 cm^{-1} for C−H stretching in cholesteryl chloroformate are present at 1462 and 2945 cm^{-1}, respectively, in chitosan-cholesterol (Figure 2). All the characteristic peaks present in chitosan-cholesterol confirmed the successful chemical conjugation of cholesterol to the chitosan backbone. Moreover, the MALDI-TOF-MS data show higher molecular mass peaks of 9551 and 9373 (compared to 5394 for chitosan) along with other low molecular weight peaks, suggesting that 8−9 cholesterols were successfully incorporated in the chitosan backbone (Figure S1).

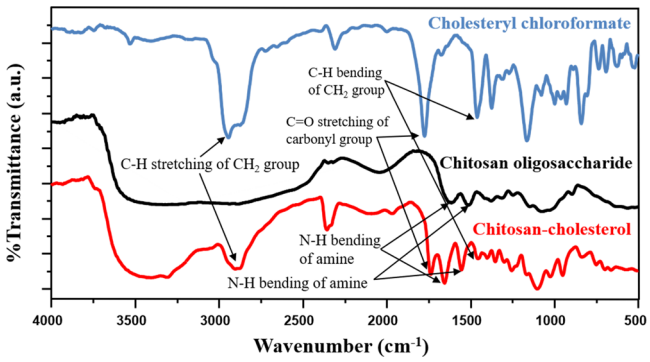

Figure 2. Characterization of chitosan-cholesterol by FTIR spectroscopy. The characteristic peak of N−H bending at 1519 and 1637 cm^{-1} of primary amine in chitosan shifted to 1552 and 1652 cm^{-1}, respectively, of amide in chitosan-cholesterol. The stretching vibration of C═O at 1770 cm^{-1} of the carbonyl group in cholesteryl chloroformate is present at 1739 cm^{-1} in chitosan-cholesterol. Moreover, peaks at 1465 cm^{-1} for C−H bending and 2949 cm^{-1} for C−H stretching in cholesteryl chloroformate present at 1462 and 2945 cm^{-1}, respectively, in chitosan-cholesterol confirmed successful conjugation of cholesterol units to the chitosan backbone.

3.2. Characterization of α-MSH Loading and Particle Size Determination of Chitosan-Cholesterol α-MSH Nanoconjugates. α-MSH loading in the chitosan-cholesterol copolymer was determined by using UV−Visible absorption spectroscopy. The characteristic absorption of α-MSH shows at 280 nm due to the presence of tryptophan residues. The same characteristics absorption at 280 nm for α-MSH was also observed for chitosan-cholesterol α-MSH nanoconjugates (Figure 3a) and due to α-MSH confirmed the successful loading of α-MSH in chitosan-cholesterol α-MSH nanoconjugates. The peak of α-MSH as shown at 280 nm in the nanoconjugates is based on the amount used during the preparation process. The drug-loading percentage was measured from the calibration curve of the free α-MSH analogue by UV−visible spectroscopy and with the help of Beer−Lambert law ($A = \varepsilon cl$). The amount of α-MSH loaded was found to be 0.25 mg/mL and the drug-loading efficiency was 35.7% (Figure S2). The size and charge of chitosan-cholesterol α-MSH polymer−drug nanoconjugates were 10−20 nm and +11.5 mV, as observed by DLS and zeta potential measurement (Figure 3b). Furthermore, to check the stability of chitosan-cholesterol α-MSH polymer−drug conjugates, we measured the size distribution (using DLS measurement) in varied concentrations of NaCl (50, 137, 200 mM) and at different time points (0, 2, and 4 h). We observed that under the experimental conditions (137 mM NaCl corresponds to the NaCl concentration of PBS and under 2 h experimental time in this article), the nanoconjugates are stable enough which could be a hallmark of good therapeutics. However, at increased NaCl concentrations with longer incubation times (300 mM, 4 h), the conjugates start to destabilize as observed from DLS size measurements (Figure S3).

3.3. Antibacterial Activity of Chitosan-Cholesterol α-MSH. Bactericidal analysis was performed using chitosan-cholesterol α-MSH polymer−drug nanoconjugates with α-MSH and chitosan-cholesterol. We have performed each assay and repeated at least thrice, and the result was interpreted in terms of percentage inhibition. The effective concentration of

https://doi.org/10.1021/acsomega.2c08209
ACS Omega 2023, 8, 12865−12877

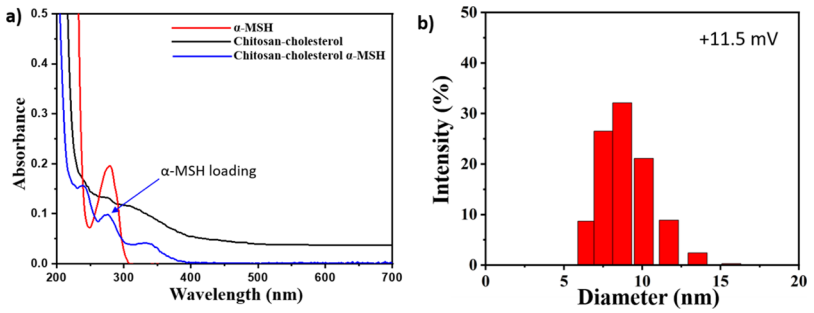

Figure 3. (a) Characterization of α-MSH loading. The characteristics peak at 280 nm under UV−Vis absorption spectroscopy confirmed the loading of α-MSH. (b) Particle size determination. The average size of chitosan-cholesterol α-MSH polymer−drug conjugates were less than 15 nm as determined by the DLS experiment with surface charge +11.5 mV.

α-MSH was 1 μM. In the case of α-MSH after two hours of treatment, we observed ∼50% inhibition of the *Staphylococcus aureus* with respect to untreated cells (i.e., 100%). The percentage of inhibition of chitosan-cholesterol was even more significant than that of α-MSH only; 21.3% of staphylococcal cells survived after the treatment which indicates that ∼79% eradication of bacterial growth occurs (Figure 4a,b). However, the chitosan-cholesterol α-MSH polymer−drug nanoconjugates have proven to be the most lethal one, where no *Staphylococcus aureus* cells were survived after two hours of treatment (inhabitation of growth was ∼100%). The result therefore predicts that the polymer−drug conjugate shows a cumulative and synergistic effect in killing of bacterial cells

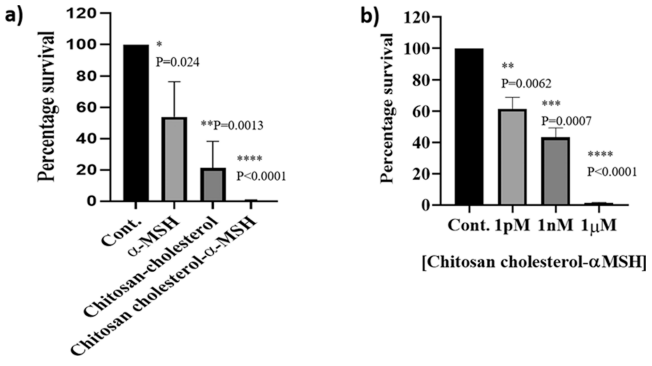

Figure 4. (a) Study of antibacterial activity: (a) Staphylococcal growth inhibition experiment was performed using chitosan-cholesterol α-MSH and individual controls. Concentration of all the components of this experiment is 1 μM. α-MSH and chitosan-cholesterol both show bacterial growth inhibition by a magnitude of 50 and 79%, respectively. The killing efficiency of the peptide conjugated was very drastic, and almost no bacterial colony was observed (∼100% inhibition) after incubation of the plate overnight. The experiment was done three times, and percentage survival was plotted using the software graph pad prism. In this calculation, the standard error of mean has been considered. Statistical analysis was done with the student *T*-Test with respect to control. All the tested sample was found to be statistically significant while the polymer peptide has the highest one $P < 0.0001$. (b) Concentration-dependent antibacterial properties of chitosan-cholesterol α-MSH. A Staphylococcal growth inhibition experiment was performed using various concentration limits of α-MSH. The concentration of α-MSH as low as 1 pM shows significant inhibition of bacterial growth (∼40% growth inhibition) of *Staphylococcus aureus*. The concentration limits around 1 nM demonstrated higher efficiency of inhibition but 1 μM shows the best efficacy. Results of all the treated samples were found to be significant; *P* value ranging from 0.0062 to lesser than 0.0001.

when it is treated in 1 μM concentration (Figure 4a). In this regard, we also compared the bactericidal efficacy of our developed chitosan-cholesterol α-MSH polymer−drug nanoconjugates when it was administered in much lower concentrations to check the effectiveness in the nanomolar and picomolar concentration range. Surprisingly, we found the efficient antibacterial activity in such smallest possible concentration ranges. The percentage of inhibition was 40% at a concentration as low as 1 pM, whereas 1 nM shows 60% killing of bacteria when it was compared with the untreated cells (Figure 4b). The result therefore indicates that chitosan-cholesterol α-MSH is a powerful antibacterial weapon that can efficiently eradicate the growth of multidrug-resistant *Staphylococcus aureus* even in the lowest possible concentration. Perhaps, these data are very important in the context of safety issues as higher concentrations produce more toxicity or side effects inside the host cell.

3.4. Analysis of the Effect of Chitosan-Cholesterol α-MSH Nanoconjugates on Growth of MRSA. Since the nanoconjugate has an inhibitory effect on *Staphylococcus aureus*, we were interested to see the effect of the following agent in the different growth phases of the opportunist pathogen. The polymer−drug nanoconjugates were treated either at the onset of the growth or during the exponential phase where the cell density steadily increases. The rationale behind it is to understand whether MRSA can restore the growth after the initial set back. Growth curve analysis shows that the growth was compromised during the initial hours where MRSA were treated with 1 and 2 μM of the polymer peptide nanoconjugates. After three hours, it started increasing and later it became almost close to the set where no treatment has been made (Figure 5). The CFU count that gives the direct number of the live cells present in the culture also indicates the same. It can therefore be predicted that the effect of the polymer−drug nanoconjugates remains for a few hours and reduced over time, which allowed the remaining cells to grow manifested by the nature of the curve. The administration of the chitosan-cholesterol α-MSH in the exponential phase (at three hour) of the growth also has some effect. The distinctive reduction was observed in the growth in the case of both sets (1 and 2 μM). The effect set aside gradually with time. Perhaps, the effect of the chitosan-cholesterol α-MSH lasts for three hours, which is evident from both types of growth analysis. It could be due to the stability of the conjugates or the cells that do not get killed by the MSH contributed in growth restoration. We aim to explore this area more in future.

3.5. Study of Morphological Changes during Bacterial Growth Inhibition. The bacterial growth inhibition

https://doi.org/10.1021/acsomega.2c08209
ACS Omega 2023, 8, 12865−12877

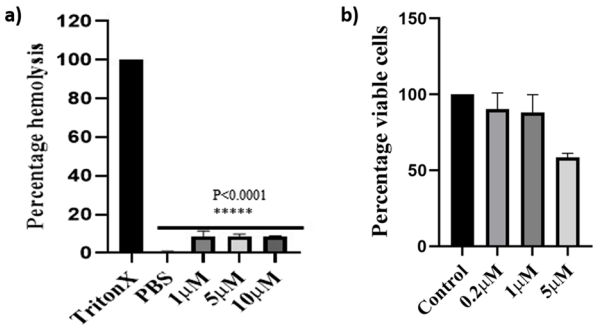

Figure 5. Growth curve analysis. (a) The growth profile of MRSA in the presence of a polymer peptide complex. Initial treatment shows retardation of growth for early three hours followed by growth enhancement in the later period. The live number of cells was calculated by CFU counts, which indicates the significant low number of live cells present in the sample treated with 1 and 2 μM of the complex. (b) Intermediate administration of the polymer peptide complex shows growth retardation for the next few hours and then becomes almost similar to the cells in the untreated sample. The number of live cells in samples with intermediate treatment does not show any significant difference as the CFU count was performed at four hours.

mechanism using chitosan-cholesterol α-MSH nanoconjugates was investigated using SEM. In order to understand the mode of interaction between chitosan-cholesterol α-MSH and *Staphylococcus aureus* in the course of bacterial growth inhibition, MRSA cells were grown up to the mid-exponential phase, and a higher number of cells (10^8) were treated with different components for two hours at 37 °C. After successful purification and extraction of the bacteria, the effect of the treatment was analyzed. In the presence of α-MSH, a fraction of the total cells has been lysed, and the formation of thread-like structures was seen under SEM (Figure 6), and cells were elongated. Actually, treatment of the α-MSH produces stress on the bacteria causing alteration of the structure. We observed that cells not only died but also the regular shape of cells changed. To have a better understanding of the effect, we performed live and death cell differentiation study with trypan blue and membrane perforation analysis by WGA that specifically stain the membrane of the bacterium. Trypan blue deposits along the membrane when the membrane is intact. Upon disruption of the membrane (cell lysis), this dye penetrates through membrane and accumulates inside the cell, which is evident in the figure (Figure 7). The treatment of the conjugates produces the lysis of the cell and therefore produces such an effect. On the other hand, the application of WGA clearly shows the perforation of the membrane structure after the treatment of the polymer−drug nanoconjugates. This is another evidence that indicates that the cell lysis is primarily vindicated by disintegration of the cell membrane. Therefore, it can be concluded that the treatment of polymer−drug nanoconjugates produces a significant damage on bacteria leading to rapid cell lysis, and cellular materials were leaked and released into the medium, causing large aggregation of numerous MRSA cells, as observed by SEM. The result correlates with our in vitro bactericidal analysis where the effect of the chitosan-cholesterol α-MSH is much more pronounced and lethal for bacterial growth inhibition and killing efficiency (Figure 6).

3.6. Toxicity Study of Nanoconjugates on Various Types of Cells Using Hemolysis Assay (RBC) and MTT Assay (Mammalian Cells). The percentage of hemolysis at different concentrations of chitosan-cholesterol α-MSH with individual controls was determined using fresh human blood samples. At various μm concentrations of α-MSH (shows the best antimicrobial activity, as shown in Figure 4a,b), the hemolysis effect is very negligible considering100% hemolysis of TritonX-100. The absorbance of the supernatant was measured at 414 nm using a 96-well plate in the multiplate reader (PerkinElmer Victor Nivo). TritonX-100 (1%) was used to measure 100% lysis of RBCs used as the positive control. Similarly, hemolysis occurs in the presence of PBS which is taken as the negative control as 0% lysis (Figure 8a). The cytotoxicity study on the human cell line also resulted in negligible toxicity under the minimum inhibitory concentrations, i.e., 0.2 and 1 μM. However, at sufficiently high concentrations of the compound (almost 8 times than MIC), it showed some effect in terms of almost 40% inhibition of the cell viability (Figure 8b). Since α-MSH was shown to inhibit melanoma cell lines (skin cancer cell line HT22) at higher concentrations, this kind of effect is possible. Perhaps, we can

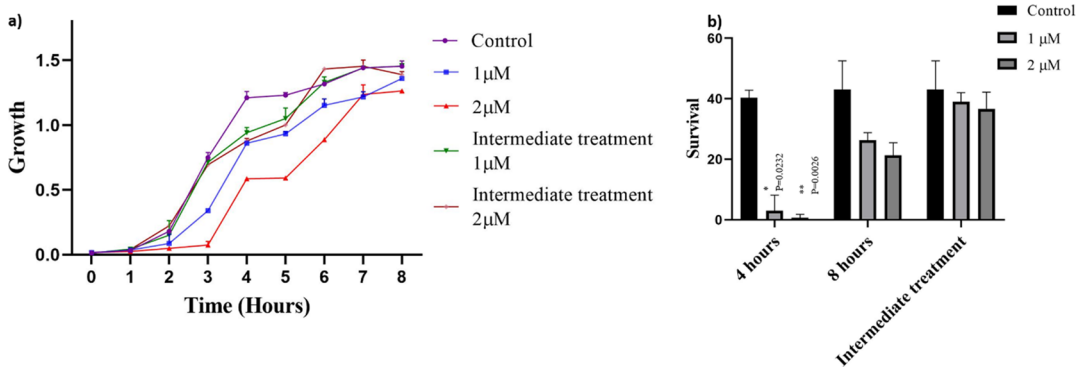

Figure 6. Study of morphological changes of *Staphylococcus aureus* after individual treatments using scanning electron micrograph: (a) the regular shape of staphylococcal cells as observed without treatment. (b) Cells changed their regular shape and formed an elongated structure after treatment of α-MSH only (c). Vigorous cell lysis was observed with concomitant release of the cellular material in the nearby medium after treatment of chitosan-cholesterol α-MSH, which results in the aggregation of the bacterial cells. (d) Magnification image of Figure 6c showing the lysis and clear aggregation of *Staphylococcus aureus*. All images were observed under 3−4 μm resolution. All the above figures are associated with the scale bar showing relative dimensions. The magnified part of figure c is shown as figure d showing cell lysis and subsequent release of cellular materials.

https://doi.org/10.1021/acsomega.2c08209
ACS Omega 2023, 8, 12865−12877

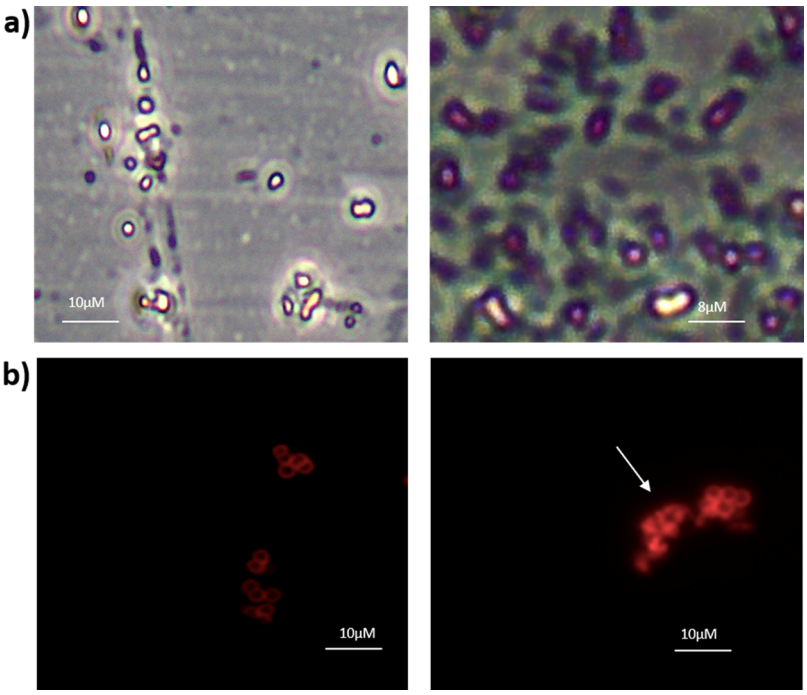

Figure 7. Cell viability analysis. (a) Cell viability assay was performed by the trypan blue staining method. The control (left most panel) shows live cells where the membrane was stained with trypan blue but the cytosol remains unstained. Polymer−drug conjugate-treated cells are lysed and therefore capable of taking stain inside the cell (right hand pane). (b) Staining with wheat germ agglutinin clearly shows the intact membrane morphology in control, whereas the treated cells show the perforated, disintegrated cell structure associated with normal healthy cells. The pore formation on the membrane is shown by an arrow. All the measurements have been taken in 100× resolution.

concentrate on the permissible dose of the chitosan-cholesterol α-MSH which is effective on the MRSA and at the same time nontoxic to blood cells and in vivo systems (Figure 8b).

4. DISCUSSION

4.1. Formulation Properties of Generated Chitosan-Cholesterol α-MSH. We used chitosan-based nanocarriers for the conjure antibacterial effect of α-MSH. We choose chitosan particularly for several reasons; the positively charged chitosan is the key for bacterial cell wall (which is negative charged) penetration and efficient cellular delivery of α-MSH. This interaction promotes destabilization and changes membrane permeability, leading to the lysis of the bacteria cell.[46] This positive charge of chitosan arises from the presence of numerous primary amine groups ($-NH_2$). According to our calculation, it has been determined that a single chitosan polymer possesses 30 number of $-NH_2$ functional group which offers enough possibility for further modifications of the base polymer (i.e., chitosan chain). We have again emphasized on easy, single-step, one-pot functionalization methods and chosen the reactive acid chloride form of cholesterol (i.e., cholesteryl chloroformate) for the current study. The reaction between chitosan and cholesteryl chloroformate is very spontaneous without addition of further reagents. Particularly, this easy way of polymer modifications will extremely help biologists and other researchers of various areas to follow similar strategies. Moreover, the chitosan is an active biopolymer that has inherent anti-bactericidal activity, as shown in previous reports.[47−54] Cholesterol which is biocompatible has made an additional key feature.[55,56] We have modified chitosan chains with various ratios of cholesterol using our developed method. However, we observed that the presence of very high ratios of cholesterol in the chitosan backbone (chitosan-cholesterol 1:15, 1:20, 1:25, or 1:30) decreases the water solubility of the chitosan-cholesterol polymer which restricts them from being used for further antibacterial applications, whereas the presence of low ratios of cholesterol in the chitosan backbone (chitosan-cholesterol 1:1, 1:3, 1:5) offers low drug-loading percentage. Therefore, we have used an optimal chitosan-cholesterol ratio of 1:8 for our study which has enough water solubility and drug-loading capacity to serve the purpose. We have purposefully chosen the chloroformate derivative of cholesterol because of its very high reactivity (as mentioned above) and we assume the full conversion as the molar ratio with the primary amine of chitosan and cholesteryl chloroformate we used. Actually, from MALDI-TOF-MS data, we have observed that 8−9 ratios of cholesterol are attached with the chitosan backbone (Figure S1), which supports our hypothesis. In the chitosan-cholesterol graft copolymer, the remaining positive charge of chitosan from $-NH_2$ (i.e., from remaining 22 no.) with the highly hydrophobic nature of cholesterol present in chitosan-cholesterol fosters the loading of negatively charged and hydrophobic drugs more by means of various nonbonding interactions (for instance Coulombic interactions, hydrophobic−hydrophobic interactions, etc.).[44] Here, the mechanism involved physical interactions between polymers and drugs to form chitosan-cholesterol α-MSH polymer−drug conjugates. The whole process of drug loading includes two types of interactions: Coulombic interactions and hydrophobic−hydrophobic interactions (not covalent interactions). Moreover, we have designed α-MSH in such a way that the overall charge is negative (−6 unit) and they have few hydrophobic amino acid residues (V, Y, W, M, F). Since the α-MSH is negatively charged, it interacts with the positively charged chitosan backbone via Coulombic interactions and the

https://doi.org/10.1021/acsomega.2c08209
ACS Omega 2023, 8, 12865−12877

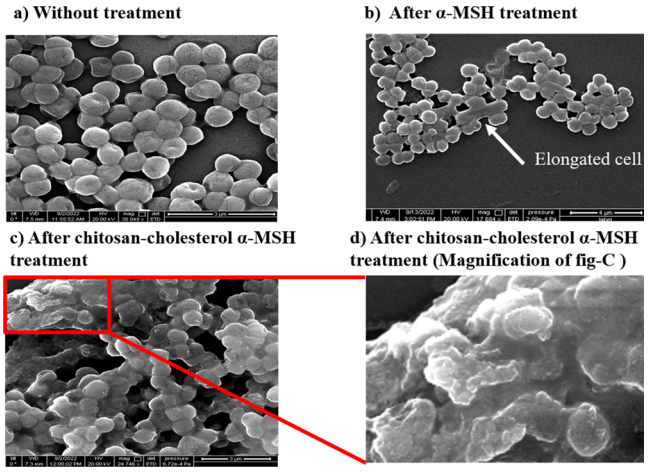

Figure 8. Effect of nanoconjugates on different types of cells. (a) Hemolytic analysis. The percentage of hemolysis at different concentrations of chitosan-cholesterol α-MSH with individual controls was determined using fresh human blood samples. At various μM concentrations of α-MSH (shows the best antimicrobial activity as shown in Figure 4a,b), the hemolysis effect is very negligible considering 100% hemolysis of TritonX-100. The absorbance of the supernatant was measured at 414 nm using a 96-well plate in a multiplate reader (PerkinElmer Victor Nivo). TritonX-100 (1%) was used to measure 100% lysis of RBC used as the positive control. Similarly, hemolysis in the presence of PBS is taken as the negative control (0% lysis). Statistical analysis was done with the student *T*-Test and the treated sample was compared with the control. (b) Mammalian cell cytotoxicity assay: furthermore, to check the cytotoxicity of chitosan-cholesterol α-MSH polymer−drug nanoconjugates, we measured cytotoxicity in HT22 cell lines using MTT assay at different concentrations of samples (0.5, 1, and 5 μM) for 2 h incubation time. We observed that the conjugates are negligible and cytotoxic to mammalian cells. However, at sufficiently high concentrations of the compound (almost 8 times than MIC), it showed some effect in terms of almost 40% inhibition of the cell viability since α-MSH was shown to inhibit the melanoma cell line (skin cancer cell line HT22) at higher concentrations.

presence of hydrophobic residues interacts via hydrophobic−hydrophobic interactions with the cholesterol molecule present in the polymer. The overall design also helps the formulation to interact with bacterial cell walls and to show efficient antibacterial activity.

4.2. Antibacterial Activity of Generated Polymer-Drug Nanoconjugates. Various studies have been demonstrated to show the utility of biopharmaceutics like peptide drugs on antimicrobial therapy for clinical importance.[6,8,12,57,58] Despite their promising role as therapeutics, their chemical stability in biological fluids with susceptibility to protease digestion, inability to maintain innate folding structures, poor selectivity, and binding specificity often limit their clinical applications.[59,60] However, their formulation in a nanocarrier not only ensures its stability but also improves the functionality of α-MSH as AMP.[61] α-MSH has already been well known for its different biological functions. This neuropeptide has immense effect in combating inflammatory response by either suppressing the effect of pro-inflammatory citokines[68] or promoting the action of anti-inflammatory citokines. As a neuropeptide, it has vast clinical applications in neurological diseases such as dementia and Alzheimer's disease.[69,72] In most cases, the dose of the administered peptide occurs in a nanomolar range.[68] Unfortunately, in the case of its application in microbial killing, the effective concentration ranges in the micromolar range which is higher than its effective dose in combating neuroinflammation. To improve the efficacy of the peptide, we conjugated it with polymer−drug conjugates which have a definite antimicrobial role. Chitosan is an active biopolymer that has inherent antibactericidal activity shown previously.[9−11,57a] The synergic effect of α-MSH and chitosan in chitosan-cholesterol α-MSH nanoconjugates was so significant that we could hardly see any bacterial colony. Even in the lowest possible (i.e., picomolar) concentration, the efficiency of the inhibition of bacterial growth was about 40%, which indicates the true potential of the developed polymer−drug nanoconjugates. Probably, the positive charge of chitosan helps α-MSH to efficiently adhere to the bacterial cell surface so that the α-MSH can make sufficient pore formation on the cell wall, leading to the extensive damage and lysis of the cell (Table 1).[12,62−67] Interestingly, the same formulation does not work that efficiently in Gram-negative *Pseudomonas aeruginosa* (Figure S5). Perhaps, the thick outer membrane of the Gram-negative bacteria prevents the efficient adherence of the nanoconjugates, resulting in the lower bactericidal activity (up to 20−25% compared to the control). Since α-MSH has already been shown to have major bactericidal activity on Gram-negative *E. coli*, fungus *C. albicans*, the manipulation of the nanoconjugates structure can render a better effect. The SEM micrograph indicates the rapid lysis of cells with subsequent release of the cellular material in the outside medium. Probably, there are other secondary mechanisms that can also play in the course of cell destruction. These include the change in membrane potential causing passive diffusion of different materials from a nearby medium to the cytoplasm, causing imbalance of the solute within cytoplasmic milieu. The probability of reactive oxygen species (ROS) generation can also come into play as there are instances of ROS-mediated cytotoxicity seen in different systems. However, in our current study, it is difficult to predict whether the polymer−drug nanoconjugates can target specialized cellular organelles that perform a distinct cellular function (e.g., ribosomes in protein synthesis, etc.). The possibility of these killing mechanisms will be investigated in the future correspondence. Moreover, in our future experiments, we will work on cross-linked polymer−drug conjugates (using glutaraldehyde, etc. as simple cross-linkers), which will enable us to report more robust nanoconjugates for performing longer-time and rigorous biological processes and therefore should be stable enough to be protected against the attack of proteases.

Safety issues of using a nanodrug formulation are very important for further consideration in clinical applications. Our investigation shows that chitosan-cholesterol α-MSH is significantly nontoxic in a wide range of concentrations in terms of its reactivity with RBCs. Moreover, the cytotoxicity study on human cells shows that the effect of the polymer−drug nanoconjugates is really negligible. Therefore, the polymer−drug nanoconjugate is stable in nature and specific in its function; it can be used for various hematological complications and other uses. The implication of this is multifaceted. Different drugs can be used with the chitosan-cholesterol-based nanoconjugates, which might be injected directly into the bloodstream in order to treat a wide range of diseases. This ensures better access of the drug or peptide molecules to their target sites, resulting in better efficacy in eradicating diseases. Different peptides, antibiotics, or antibody

https://doi.org/10.1021/acsomega.2c08209
ACS Omega 2023, 8, 12865−12877

Table 1. Summary of Previous Reports That Relates to the Current Investigation

sl. no.	study	formulation	model used	efficiency	remarks
1.	Shireen et al.[57a]	combination of α-MSH with conventional antibiotic ampicillin.	*S. aureus* strain (ISP479C), several methicillin-sensitive (MSSA), and methicillin-resistant (MRSA *S. aureus* strains	84%	α-MSH could be an efficient candidate of a novel class of antimicrobial agents.
2.	Matsuzaki et al.[62]	magainin analogues with different charges (0 to +6) and hydrophobicity.	*Escherichia coli* (ATCC 8739), *Acinetobacter calcoaceticus* (ATCC 14987), and *Proteus vulgaris* (ATCC 1331)	not reported	an amphiphilic peptide with high basicity and low hydrophobicity could be an efficient candidate for a therapeutic agent.
3.	Rasul et al.[63]	melimine	*Pseudomonas aeruginosa* 6294 and *S. aureus* 38	35–40%	analysis of differences in the action of cationic peptides toward Gram-positive and Gram-negative bacteria promotes a refined targeting of difficult-to-treat bacterial infections.
4.	Mumtaz et al.[12]	palmitoylated analogues, Pal-α-MSH (6–13) and Pal-α-MSH (11–13), of the C-terminal fragments of α-MSH.	methicillin-sensitive *S. aureus* ATCC 29213 (MSSA) and methicillin-resistant *S. aureus* ATCC 33591 (MRSA)	99.9% (bactericidal effect = 3 log reduction in viability)	Pal-α-MSH (11–13) can be potentially used in the treatment of planktonic as well as sessile *S. aureus* infections.
5.	d'Angelo et al.[64]	PLGA nanoparticles containing a model CAMP, colistin (Col).	*P. aeruginosa* ATCC 27853	not reported	engineering of PLGA nanoparticles represents a promising approach to harness novel antimicrobials for *P. aeruginosa* infections.
6.	Yasir et al.[65]	Mel4 and its precursor peptide melimine.	*S. aureus* 31 (contact lens induced peripheral ulcer isolate), *S. aureus* 38 (microbial keratitis isolate), and the type strain of *S. aureus*, ATCC 6538 (isolated from a human lesion)	40%	cell death induced by Mel4 involves the release of autolysins and amphipathic characteristics of melimine causes disruption of the cell membranes leading to cell death.
7.	Zhang et al.[66]	DP7 (a short 12 amino acid AMP)	ATCC 25923 (MSSA), methicillin-resistant strain ATCC 33591 (MRSA), the sigB-defective strain RN4220 and *Escherichia coli* (ATCC 25922), and *Pseudomonas aeruginosa* (PAO1) strain	90% reduction in lethality of infection.	DP7 could be an efficient therapeutic for fighting *S. aureus* infections.

molecules can be conjugated with chitosan-cholesterol-based nanoconjugates to treat life-threatening diseases associated with toxins and pathogens present in the blood. Therefore, this versatile system has enormous potential as a potential delivery system in the clinical sector (Table 1).[12,62−67]

4.3. Future Plan. We have demonstrated the significant effect of α-MSH in nanodrug formulations on MRSA. In our future study, we are working to show an antibacterial effect on a series of other Gram-positive bacteria for better therapeutic screening. It could be applied to the most resistant bacterial biofilm which is the main concern for various hospital-based infections (nosocomial infection). The main advantage of our developed nanocarrier is that the chemical synthesis method is fully tunable and versatile in nature, where we can chemically conjugate a variety of cholesterol ratios and choose a wide range of AMPs according to the aim. Moreover, in our future study, we are working on negatively charged polymers (−CO_2H, −OH functionalized; e.g., alginate, dextran, PEG, amino acid-based block copolymers, etc.) to cover the full spectrum of AMPs with negative, positive, and zero charges and according to requirements. Additionally, multiple drugs (similar or different types; small molecule, peptide, antibiotic, etc.) could be loaded with it that provides docking sites for antimicrobial substances. This particular system is congruent when we are working against multidrug-resistant bacterial systems that require applications of more than one antibiotic simultaneously. It can be administered to the biofilm formed by different Gram-positive and -negative bacteria which is the trademark of rendering antibiotic resistance. This biofilm plays a vital role in spreading all sorts of secondary infections in the hospital sector and needs to be targeted for combating pathogenesis in critical patients. The versatile chemical composition of this nanoconjugated peptide or antibiotic should be easily interacted with the exterior part of the biofilm helping in penetrating the drug (antibiotic) or peptide into the core where it can be exposed to the pathogen and destroy it. Penetration of the drug into the biofilm is a real problem that makes those biofilm-forming bacteria (ESKAPE organism) so difficult to treat with, and this problem can be circumvented using this nanoconjugated system. Additionally, the chitosan-cholesterol system provides additional chemical stability which can be effective for Gram-negative bacteria widely found in infections. After all, this multifaceted nanocarrier has the potential to be used as an important alternative therapy for various types of multidrug-resistant bacteria with a wide opportunity of AMPs. Finally, the mechanistic aspects of cell lysis and how the cellular organelles take part with it after applying the formulations will be studied very extensively.

5. CONCLUSIONS

We generated a cholesterol-grafted chitosan copolymer (chitosan-cholesterol) by using a simple, one-pot chemical modification technique. The developed chitosan-cholesterol is positively charged and amphiphilic in nature and is used to load α-MSH, an endogenous neuropeptide, and thus prepare chitosan-cholesterol α-MSH polymer−drug nanoconjugates. The drug loading percentage was significantly high (35.7%). The bactericidal analysis using 1 μM concentration of α-MSH in *Staphylococcus aureus* after two hours of treatment shows 50 and 79% eradication of bacterial growth for α-MSH and chitosan-cholesterol with respect to untreated cells (i.e., 100%), respectively. However, chitosan-cholesterol α-MSH shows almost no survival of bacterial colony. However, the

https://doi.org/10.1021/acsomega.2c08209
ACS Omega 2023, 8, 12865−12877

chitosan-cholesterol α-MSH polymer−drug nanoconjugates have proven to be the most lethal ones. The result therefore predicts that the polymer−drug conjugate shows a synergic effect on inhibition of bacterial cell growth when it is treated in 1 μM concentration. Furthermore, chitosan-cholesterol α-MSH polymer−drug nanoconjugates exhibit profound antibacterial properties in the concentration limit as low as picomolar concentration with 60% inhibition which implies to be a powerful tool for effective and efficient antibacterial therapy. Our SEM-based study clearly revealed that the lethal effect of pore formation on the cell wall and release of the cellular materials into the medium result in large aggregation of numerous cells. Our development of chitosan-based tunable and versatile nanocarriers could be widely applied for both Gram-positive and Gram-negative bacterial systems with a broad spectrum of different types of drugs to combat multidrug resistance.

■ ASSOCIATED CONTENT

Supporting Information

The Supporting Information is available free of charge at https://pubs.acs.org/doi/10.1021/acsomega.2c08209.

MALDI-TOF-MS of chitosan-cholesterol; calibration curve of α-MSH and determination of loading percentage; stability of chitosan-cholesterol α-MSH polymer−drug conjugates; chart showing MIC of polymer−drug nanoconjugates on MRSA; cell killing analysis of *Pseudomonas aeruginosa*; and Resazurin experiment (PDF)

■ AUTHOR INFORMATION

Corresponding Authors

Arnab Basu − *Department of Biomedical Science and Technology, The School of Biological Sciences, Ramakrishna Mission Vivekananda Educational Research Institute, Howrah, West Bengal 711202, India;* orcid.org/0000-0002-8048-8733; Email: arnab.basu@gm.rkmvu.ac.in

Amit Ranjan Maity − *Amity Institute of Biotechnology, Amity University, Kolkata, West Bengal 700135, India;* orcid.org/0000-0002-5253-3680; Email: armaity@kol.amity.edu

Authors

Sourav Barman − *Amity Institute of Biotechnology, Amity University, Kolkata, West Bengal 700135, India*

Asmita Chakraborty − *Department of Biomedical Science and Technology, The School of Biological Sciences, Ramakrishna Mission Vivekananda Educational Research Institute, Howrah, West Bengal 711202, India*

Sujata Saha − *Department of Biomedical Science and Technology, The School of Biological Sciences, Ramakrishna Mission Vivekananda Educational Research Institute, Howrah, West Bengal 711202, India*

Kunal Sikder − *Department of Biomedical Science and Technology, The School of Biological Sciences, Ramakrishna Mission Vivekananda Educational Research Institute, Howrah, West Bengal 711202, India*

Sayoni Maitra Roy − *Amity Institute of Biotechnology, Amity University, Kolkata, West Bengal 700135, India*

Barkha Modi − *Department of Biomedical Science and Technology, The School of Biological Sciences, Ramakrishna Mission Vivekananda Educational Research Institute, Howrah, West Bengal 711202, India*

Sabarnee Bahadur − *Department of Biomedical Science and Technology, The School of Biological Sciences, Ramakrishna Mission Vivekananda Educational Research Institute, Howrah, West Bengal 711202, India*

Ali Hossain Khan − *S. N. Bose National Centre for Basic Sciences, Kolkata, West Bengal 700106, India;* orcid.org/0000-0001-7155-0200

Dipak Manna − *Department of Biomedical Science and Technology, The School of Biological Sciences, Ramakrishna Mission Vivekananda Educational Research Institute, Howrah, West Bengal 711202, India*

Pousali Bag − *Amity Institute of Biotechnology, Amity University, Kolkata, West Bengal 700135, India*

Ankan Kumar Sarkar − *School of Materials Sciences, Indian Association for the Cultivation of Science, Kolkata, West Bengal 700032, India;* orcid.org/0000-0002-6486-222X

Rishi Bhattacharya − *Department of Biomedical Science and Technology, The School of Biological Sciences, Ramakrishna Mission Vivekananda Educational Research Institute, Howrah, West Bengal 711202, India*

Complete contact information is available at: https://pubs.acs.org/10.1021/acsomega.2c08209

Author Contributions

⊥S.B. and A.C. have contributed equally.

Funding

The project is financially supported by Ramalingaswami Re-entry Fellowship sponsored by the Department of Biotechnology (DBT), Government of India, reference no: BT/RLF/Re-entry/53/2019; Ramalingaswami fellowship to ARM, BT/RLF/Re-entry/43/2019; and Ramalingaswami fellowship to AB.

Notes

The authors declare no competing financial interest.

■ ACKNOWLEDGMENTS

A.R.M., A.B., and S.B. would like to acknowledge the Department of Biotechnology (DBT) for providing funding and fellowship.

■ REFERENCES

(1) Lei, J.; Sun, L.; Huang, S.; Zhu, C.; Li, P.; He, J.; Mackey, V.; Coy, D. H.; He, Q. The antimicrobial peptides and their potential clinical applications. *Am. J. Transl. Res.* **2019**, *11*, 3919−3931.

(2) Zasloff, M. Antimicrobial peptides of multicellular organisms. *Nature* **2002**, *415*, 389−395.

(3) Hancock, R. E.; Diamond, G. The role of cationic antimicrobial peptides in innate host defences. *Trends Microbiol.* **2000**, *8*, 402−410.

(4) Brogden, K. A. Antimicrobial peptides: pore formers or metabolic inhibitors in bacteria? *Nat. Rev. Microbiol.* **2005**, *3*, 238−250.

(5) Le, C. F.; Fang, C. M.; Sekaran, S. D. Intracellular targeting mechanisms by antimicrobial peptides. *Antimicrob. Agents Chemother.* **2017**, *61*, e02340−e02316.

(6) Singh, J.; Joshi, S.; Mumtaz, S.; Maurya, N.; Ghosh, I.; Khanna, S.; Natarajan, V. T.; Mukhopadhyay, K. Enhanced Cationic Charge Is a Key Factor in Promoting Staphylocidal Activity of α-Melanocyte Stimulating Hormone via Selective Lipid Affinity. *Sci. Rep.* **2016**, *6*, 31492.

(7) Chang, S.-H.; Lin, Y.-Y.; Wu, G.-J.; Huang, C.-H.; Tsai, G. J. Effect of chitosan molecular weight on anti-inflammatory activity in

the RAW 264.7 macrophage model. *Int. J. Biol. Macromol.* **2019**, *131*, 167−175.
(8) Singh, M.; Mukhopadhyay, K. C-Terminal Amino Acids of Alpha-Melanocyte-Stimulating Hormone Are Requisite for Its Antibacterial Activity against Staphylococcus Aureus. *Antimicrob. Agents Chemother.* **2011**, *55*, 1920−1929.
(9) Ahmed, S. B.; Mohamed, H. I.; Al-Subaie, A. M.; Al-Ohali, A. I.; Mahmoud, N. M. R. Investigation of the Antimicrobial Activity and Hematological Pattern of Nano-Chitosan and Its Nano-Copper Composite. *Sci. Rep.* **2021**, *11*, 9540.
(10) de Andrade, L. F.; Apolinário, A. C.; Rangel-Yagui, C. O.; Stephano, M. A.; Tavares, L. C. Chitosan Nanoparticles for the Delivery of a New Compound Active against Multidrug-Resistant Staphylococcus Aureus. *J. Drug Deliv. Sci. Technol.* **2020**, *55*, No. 101363.
(11) Scolari, I. R.; Páez, P. L.; Musri, M. M.; Petiti, J. P.; Torres, A.; Granero, G. E. Rifampicin Loaded in Alginate/Chitosan Nanoparticles as a Promising Pulmonary Carrier against Staphylococcus Aureus. *Drug Deliv. Transl. Res.* **2020**, *10*, 1403−1417.
(12) Mumtaz, S.; Behera, S.; Mukhopadhyay, K. Lipidated Short Analogue of α-Melanocyte Stimulating Hormone Exerts Bactericidal Activity against the Stationary Phase of Methicillin-Resistant *Staphylococcus Aureus* and Inhibits Biofilm Formation. *ACS Omega* **2020**, *5*, 28425−28440.
(13) Kinoh, H.; Quader, S.; Shibasaki, H.; Liu, X.; Maity, A.; Yamasoba, T.; Cabral, H.; Kataoka, K. Translational nanomedicine boosts anti-PD1 therapy to eradicate orthotopic PTEN-negative glioblastoma. *ACS Nano* **2020**, *14*, 10127−10140.
(14) Maity, A. R.; Stepensky, D. Nuclear and perinuclear targeting efficiency of quantum dots depends on density of peptidic targeting residues on their surface. *J. Controlled Release* **2017**, *257*, 32−39.
(15) Maity, A. R.; Stepensky, D. Efficient subcellular targeting to the cell nucleus of quantum dots densely decorated with a nuclear localization sequence peptide. *ACS Appl. Mater. Interfaces* **2016**, *8*, 2001−2009.
(16) Maity, A. R.; Stepensky, D. Limited efficiency of drug delivery to specific intracellular organelles using subcellularly "targeted" drug delivery systems. *Mol. Pharmaceutics* **2016**, *13*, 1−7.
(17) Maity, A. R.; Stepensky, D. Delivery of drugs to intracellular organelles using drug delivery systems: Analysis of research trends and targeting efficiencies. *Int. J. Pharm.* **2015**, *496*, 268−274.
(18) Cabra, H.; Miyata, K.; Osada, K.; Kataoka, K. Block copolymer micelles in nanomedicine applications. *Chem. Rev.* **2018**, *118*, 6844−6892.
(19) Quader, S.; Liu, X.; Toh, K.; Su, Y. L.; Maity, A. R.; Tao, A.; Paraiso, W. K. D.; Mochida, Y.; Kinoh, H.; Cabral, H.; Kataoka, K. Supramolecularly enabled pH-triggered drug action at tumor microenvironment potentiates nanomedicine efficacy against glioblastoma. *Biomaterials* **2021**, *267*, No. 120463.
(20) (68.) Roy, S. M.; Garg, V.; Barman, S.; Ghosh, C.; Maity, A. R.; Ghosh, S. K. Kinetics of nanomedicine in tumor spheroid as an in vitro model system for efficient tumor-targeted drug delivery with insights from mathematical models. *Front. Bioeng. Biotechnol.* **2021**, *9*, No. 785937.
(21) Zhang, X.; Chen, X.; Zhao, Y. Nanosystems for Immune Regulation against Bacterial Infections: A Review. *ACS Appl. Nano Mater.* **2022**, *5*, 13959−13971.
(22) Karimifard, S.; Rezaei, N.; Jamshidifar, E.; Moradi, F. L. S.; Abdihaji, M.; Mansouri, A.; Hosseini, M.; Ahmadkhani, N.; Rahmati, Z.; Heydari, M.; Vosough, M. pH-Responsive Chitosan-Adorned Niosome Nanocarriers for Co-Delivery of Drugs for Breast Cancer Therapy. *ACS Appl. Nano Mater.* **2022**, *5*, 8811−8825.
(23) Wang, C.; Yang, Y.; Cao, Y.; Liu, K.; Guo, X.; Liu, W.; Hao, R.; Song, H.; Zhao, R. Nanocarriers for the delivery of antibiotics into cells against intracellular bacterial infection. *Biomater. Sci.* **2023**, *11*, 432−444.
(24) Pelgrift, R. Y.; Friedman, A. J. Nanotechnology as a therapeutic tool to combat microbial resistance. *Adv. Drug Delivery Rev.* **2013**, *65*, 1803−1815.
(25) Khan, S. T.; Musarrat, J.; Al-Khedhairy, A. A. Countering drug resistance, infectious diseases, and sepsis using metal and metal oxides nanoparticles: current status. *Colloids Surf., B* **2016**, *146*, 70−83.
(26) Zhang, Y.; Li, P.; Su, R.; Wen, F.; Jia, Z.; Lv, Y.; Cai, J.; Su, W. Curcumin-loaded multifunctional chitosan gold nanoparticles: An enhanced PDT/PTT dual modalphototherapeutic and pH-responsive antimicrobial agent. *Photodiagn. Photodyn. Ther.* **2022**, *39*, No. 103011.
(27) Zazo, H.; Colino, C. I.; Lanao, J. M. Current applications of nanoparticles in infectious diseases. *J. Controlled Release* **2016**, *224*, 86−102.
(28) Zhang, J.; Zhang, F.; Hu, X.; Yang, J.; Wang, H.; Durrani, S.; Wu, F. G.; Lin, F. Self-Assembly and Disassembly of Glycol Chitosan/Photosensitizer Nano-Micelles for Antibacterial Photodynamic Therapy. *ACS Appl. Polym. Mater.* **2022**, *4*, 8665−8675.
(29) Yu, H. T.; Zhang, J. Q.; Sun, M. C.; Chen, H.; Shi, X. M.; You, F. P.; Qiao, S. Y. Polymeric Nanohybrids Engineered by Chitosan Nanoparticles and Antimicrobial Peptides as Novel Antimicrobials in Food Biopreservatives: Risk Assessment and Anti-Foodborne Pathogen *Escherichia coli* O157:H7 Infection by Immune Regulation. *J. Agric. Food Chem.* **2022**, *70*, 12535−12549.
(30) Mansoor, B.; Li, S.; Chen, W. Highly efficient antifogging/antimicrobial dual-functional chitosan based coating for optical devices. *Carbohydr. Polym.* **2022**, *296*, No. 119928.
(31) Zhang, C.; Zhao, W.; Bian, C.; Hou, X.; Deng, B.; McComb, D. W.; Chen, X.; Dong, Y. Antibiotic-Derived Lipid Nanoparticles to Treat Intracellular Staphylococcus aureus. *ACS Appl. Bio Mater.* **2019**, *2*, 1270−1277.
(32) Liu, Y.; Sun, M.; Wang, T.; Chen, X.; Wang, H. Chitosan-based self-assembled nanomaterials: Their application in drug delivery. *View* **2021**, *2*, No. 2020069.
(33) Zhang, J.; Yang, Z.; Li, Y. H.; Durrani, S.; Pang, A. P.; Gao, Y.; Wu, F. G.; Lin, F. Super-Stable Chitosan-Based Nanoparticles for Broad Spectrum Antimicrobial Photodynamic Therapy. *ACS Appl. Polym. Mater.* **2021**, *1*, 425−434.
(34) Haktaniyan, M.; Bradley, M. Polymers showing intrinsic antimicrobial activity. *Chem. Soc. Rev.* **2022**, *51*, 8584−8611.
(35) Zhao, L.-M.; Shi, L.-E.; Zhang, Z.-L.; Chen, J.-M.; Shi, D.-D.; Yang, J.; Tang, Z.-X. Preparation and application of chitosan nanoparticles and nanofibers. *Braz. J. Chem. Eng.* **2011**, *28*, 353−362.
(36) Karimi-Soflou, R.; Karkhaneh, A.; Shabani, I. Size-adjustable self-assembled nanoparticles through microfluidic platform promotes neuronal differentiation of mouse embryonic stem cells. *Biomater. Adv.* **2022**, *140*, No. 213056.
(37) Cavallaro, G.; Micciulla, S.; Chiappisi, L.; Lazzara, G. Chitosan-based smart hybrid materials: A physico-chemical perspective. *J. Mater. Chem.* **2021**, *9*, 594−611.
(38) Matica, M. A.; Aachmann, F. L.; Tøndervik, A.; Sletta, H.; Ostafe, V. Chitosan as a Wound Dressing Starting Material: Antimicrobial Properties and Mode of Action. *Int. J. Mol. Sci.* **2019**, *20*, 5889.
(39) Kong, M.; Chen, X. G.; Xing, K.; Park, H. J. Antimicrobial Properties of Chitosan and Mode of Action: a state of the art review. *Int. J. Food Microbiol.* **2010**, *144*, 51−63.
(40) Jana, S., Jana, S., Eds. Functional Chitosan: Drug Delivery and Biomedical Applications. *Functional chitosan*, 2019, vol *1*; pp 1−489.
(41) Hu, Y.; Du, Y.; Yang, J.; Tang, Y.; Li, J.; Wang, X. Self-Aggregation and Antibacterial Activity of N-Acylated Chitosan. *Polymer* **2007**, *48*, 3098−3106.
(42) Tikhonov, V. E.; Stepnova, E. A.; Babak, V. G.; Yamskov, I. A.; Palma-Guerrero, J.; Jansson, H.-B.; Lopez-Llorca, L. V.; Salinas, J.; Gerasimenko, D. V.; Avdienko, I. D.; Varlamov, V. P. Bactericidal and Antifungal Activities of a Low Molecular Weight Chitosan and Its N−/2(3)- (Dodec-2-Enyl) Succinoyl/-Derivatives. *Carbohydr. Polym.* **2006**, *64*, 66−72.
(43) Yinsong, W.; Lingrong, L.; Jian, W.; Zhang, Q. Preparation and characterization of self-aggregated nanoparticles of cholesterol-modified O-carboxymethyl chitosan conjugates. *Carbohydr. Polym.* **2007**, *69*, 597−606.

https://doi.org/10.1021/acsomega.2c08209
ACS Omega 2023, 8, 12865−12877

(44) Maity, A. R.; Jana, N. R. Chitosan− Cholesterol-Based Cellular Delivery of Anionic Nanoparticles. *J. Phys. Chem. C* **2011**, *115*, 137−144.
(45) Shireen, T.; Singh, M.; Dhawan, B.; Mukhopadhyay, K. Characterization of Cell Membrane Parameters of Clinical Isolates of Staphylococcus Aureus with Varied Susceptibility to Alpha-Melanocyte Stimulating Hormone. *Peptides* **2012**, *37*, 334−339.
(46) Machul, A.; Mikołajczyk, D.; Regiel-Futyra, A.; Heczko, P. B.; Strus, M.; Arruebo, M.; Stochel, G.; Kyzioł, A. Study on inhibitory activity of chitosan-based materials against biofilm producing Pseudomonas aeruginosa strains. *J. Biomater. Appl.* **2015**, *30*, 269−278.
(47) Divya, K.; Vijayan, S.; George, T. K.; Jisha, M. S. Antimicrobial Properties of Chitosan Nanoparticles: Mode of Action and Factors Affecting Activity. *Fibers Polym.* **2017**, *18*, 221−230.
(48) Yilmaz Atay, H. Antibacterial Activity of Chitosan-Based Systems. In *Functional Chitosan*, 2019, vol *1*; pp 457−489.
(49) Qin, C.; Li, H.; Xiao, Q.; Liu, Y.; Zhu, J.; Du, Y. Water-Solubility of Chitosan and Its Antimicrobial Activity. *Carbohydr. Polym.* **2006**, *63*, 367−374.
(50) Yen, M.-T.; Yang, J.-H.; Mau, J.-L. Antioxidant properties of chitosan from crab shells. *Carbohydr. Polym.* **2008**, *74*, 840−844.
(51) Goy, R. C.; Morais, S. T. B.; Assis, O. B. G. Evaluation of the Antimicrobial Activity of Chitosan and Its Quaternized Derivative on *E. coli* and *S. aureus* Growth. *Rev. Bras. Farmacogn.* **2016**, *26*, 122−127.
(52) Bangun, H.; Tandiono, S.; Arianto, A. Preparation and Evaluation of Chitosan-Tripolyphosphate Nanoparticles Suspension as an Antibacterial Agent. *J. Appl. Pharm. Sci.* **2018**, *8*, 147−156.
(53) Costa, E. M.; Silva, S.; Vicente, S.; Neto, C.; Castro, P. M.; Veiga, M.; Madureira, R.; Tavaria, F.; Pintado, M. M. Chitosan Nanoparticles as Alternative Anti-Staphylococci Agents: Bactericidal, Antibiofilm and Antiadhesive Effects. *Mater. Sci. Eng., C* **2017**, *79*, 221−226.
(54) Fahimirad, S.; Ghaznavi-Rad, E.; Abtahi, H.; Sarlak, N. Antimicrobial Activity, Stability and Wound Healing Performances of Chitosan Nanoparticles Loaded Recombinant LL37 Antimicrobial Peptide. *Int. J. Pept. Res. Ther.* **2021**, *27*, 2505−2515.
(55) Jong, T.; Mudgil, P. Exploring antimicrobial properties of cholesterol esters: a systematic literature review. *All Life* **2022**, *15*, 684−691.
(56) Zhang, R.; Wu, F.; Wu, L.; Tian, Y.; Zhou, B.; Zhang, X.; Huang, R.; Yu, C.; He, G.; Yang, L. Novel Self-Assembled Micelles Based on Cholesterol-Modified Antimicrobial Peptide (DP7) for Safe and Effective Systemic Administration in Animal Models of Bacterial Infection. *Antimicrob. Agents Chemother.* **2018**, *62*, No. e00368-18.
(57) (a) Madhuri; Shireen, T.; Venugopal, S. K.; Ghosh, D.; Gadepalli, R.; Dhawan, B.; Mukhopadhyay, K. In Vitro Antimicrobial Activity of Alpha-Melanocyte Stimulating Hormone against Major Human Pathogen *Staphylococcus Aureus*. *Peptides* **2009**, *30*, 1627−1635. (b) Marqus, S.; Pirogova, E.; Piva, T. J. Evaluation of the use of therapeutic peptides for cancer treatment. *J. Biomed. Sci.* **2017**, *24*, 21.
(58) Weinstock, M. T.; Francis, J. N.; Redman, J. S.; Kay, M. S. Protease-resistant peptide design-empowering nature's fragile warriors against HIV. *Biopolymers* **2012**, *98*, 431−442.
(59) Klein, M. Stabilized helical peptides: overview of the technologies and its impact on drug discovery. *Expert Opin. Drug Discov.* **2017**, *12*, 1117−1125.
(60) Pal, I.; Bhattacharyya, D.; Kar, R. K.; Zarena, D.; Bhunia, A.; Atreya, H. S. A Peptide-Nanoparticle System with Improved Efficacy against Multidrug Resistant Bacteria. *Sci. Rep.* **2019**, *9*, 4485.
(61) Chávez de Paz, L. E.; Resin, A.; Howard, K. A.; Sutherland, D. S.; Wejse, P. L. Antimicrobial Effect of Chitosan Nanoparticles on Streptococcus Mutans Biofilms. *Appl. Environ. Microbiol.* **2011**, *77*, 3892−3895.
(62) Matsuzaki, K.; Sugishita, K. I.; Harada, M.; Fujii, N.; Miyajima, K. Interactions of an antimicrobial peptide, magainin 2, with outer and inner membranes of Gram-negative bacteria. *Biochim. Biophys. Acta, Biomembr.* **1997**, *1327*, 119−130.
(63) Rasul, R.; Cole, N.; Balasubramanian, D.; Chen, R.; Kumar, N.; Willcox, M. D. P. Interaction of the antimicrobial peptide melimine with bacterial membranes. *Int. J. Antimicrob. Agents* **2010**, *35*, 566−572.
(64) d'Angelo, I.; Casciaro, B.; Miro, A.; Quaglia, F.; Mangoni, M. L.; Ungaro, F. Overcoming barriers in Pseudomonas aeruginosa lung infections: Engineered nanoparticles for local delivery of a cationic antimicrobial peptide. *Colloids Surf., B* **2015**, *135*, 717−725.
(65) Yasir, M.; Dutta, D.; Willcox, M. D. Mode of action of the antimicrobial peptide Mel4 is independent of Staphylococcus aureus cell membrane permeability. *PLoS One* **2019**, *14*, No. e0215703.
(66) Zhang, R.; Wang, Z.; Tian, Y.; Yin, Q.; Cheng, X.; Lian, M.; Yang, L. Efficacy of antimicrobial peptide DP7, designed by machine-learning method, against methicillin-resistant Staphylococcus aureus. *Front. Microbiol.* **2019**, *10*, 1175.
(67) Manna, S. K.; Aggarwal, B. B. α-melanocyte-stimulating hormone inhibits the nuclear transcription factor NF-κB activation induced by various inflammatory agents. *J. Immunol.* **1998**, *161*, 2873−2880.
(68) Leone, S.; Noera, G.; Bertolini, A. Melanocortins as innovative drugs for ischemic diseases and neurodegenerative disorders: established data and perspectives. *Curr. Med. Chem.* **2013**, *20*, 735−750.
(69) Ma, K.; McLaurin, J. α-melanocyte stimulating hormone prevents GABAergic neuronal loss and improves cognitive functions in Alzheimer's disease. *J. Neurosci.* **2014**, *34*, 6736−6745.

https://doi.org/10.1021/acsomega.2c08209
ACS Omega 2023, 8, 12865−12877